D. This is followed by overexpansion to pressures below the freestream. Strength of the initial shock is gradually attenuated due to its interaction with the boundary layers and the shape of the nacelle outer surface. Although the linear theory of Ref. 4 was adequate for predicting pressure signatures near an isolated nacelle, the pressure coefficient distribution on the flat plate using Ref. 4 illustrates the limitation of the linear theory for this configuration. An overexpansion to pressure below the freestream occurs downstream of location E where the nacelle lip shock impinges on the flat plate. Other shock reflections on the flat plate are not predicted. The interference pressures between the flat plate and the nacelle at $M_\infty = 1.6$ and 2.0 are similar to those observed at $M_\infty = 2.3$. However, the incident and reflected shock structure appears to be more complicated at $M_\infty = 1.6$ where some of the reflected shocks resemble normal shocks. The pressure distributions on the flat plate illustrate the lift induced on the flat plate by the nacelle. The normal force coefficient C_N on the flat plate is computed at each freestream Mach number. The values of C_N at $M_\infty = 1.6$, 2.0, and 2.3 are 0.026, 0.32, and 0.035, respectively. A reflexed wing can certainly reduce the negative pressure gradient on the inboard side and take advantage of the positive pressure gradient created due to the interference.

Concluding Remarks

Three-dimensional flows past an isolated nacelle and a nacelle in close proximity to a flat plate were computationally simulated. This was accomplished by solving the Navier–Stokes equations by an implicit, upwind-biased, finite volume method. The computational grids were generated using a hybrid domain decomposition technique. A multiblock grid was used for the isolated nacelle case. For the nacelle-flat plate case, both multiblock and grid overlapping techniques were utilized for easing the grid generation task for this complex configuration. The results indicated the significant limitations of the linearized method for accurately predicting the mutual interference between the components. The effects of Mach number on such flowfields were also investigated and are presented in the present study.

Acknowledgments

This work is supported under NASA Contract NAS1-19000. The Technical Monitor is C. M. Darden.

References

[1]Harris, R. V., Jr., "A Numerical Technique for Analysis of Wave Drag at Lifting Conditions," NASA TN D-3586, Oct. 1966.

[2]Carlson, H. W., and Miller, D. S., "Numerical Methods for the Design and Analysis of Wings at Supersonic Speeds," NASA TN D-7713, Dec. 1974.

[3]Carlson, H. W., and Mack, R. J., "Estimation of Wing Nonlinear Aerodynamic Characteristics at Supersonic Speeds," NASA TP-1718, Nov. 1980.

[4]Mack, R. J., "A Numerical Method for Evaluation and Utilization of Supersonic Nacelle-Wing Interference," NASA TN D-5057, March 1969.

[5]Middelton, W. D., and Lundry, J. L., "A Computational System for Aerodynamic Design and Analysis of Supersonic Aircraft. Part 1—General Description and Theoretical Development," NASA CR-2715, July 1976.

[6]Whitham, G., "The Flow Pattern of a Supersonic Projectile," *Communication on Pure and Applied Mathematics*, Vol. V, No. 3, 1952, pp. 301–348.

[7]Walkden, F., "The Shock Pattern of a Wing-Body Combination, Far from the Flight Path," *Aeronautical Quarterly*, Vol. IX, Pt. 2, 1985, pp. 164–194.

[8]Hayes, W., Haefeli, R., and Kulsrud, H., "Sonic-Boom Propagation in a Stratified Atmosphere, with a Computer Program," NASA CR-1299, April 1969.

[9]Baysal, O., Fouladi, K., and Lessard, V. R., "A Multigrid Method to Solve 3-D Viscous Equations on Overlapped and Embedded Grids," *AIAA Journal*, Vol. 29, No. 6, 1991, pp. 903–910.

[10]Fouladi, K., and Baysal, O., "Viscous Simulation Method for Unsteady Flows Past a Configuration with Nonsimilar Multicomponents," *Journal of Fluids Engineering*, Vol. 114, No. 1, 1992, pp. 161–169.

[11]Fouladi, K., Baysal, O., and Newman, J. C., "Hybrid Domain Decomposition for Configurations with Multiple Nonsimilar Components," SIAM 5th Conf. on Domain Decomposition Methods for Partial Differential Equations, Norfolk, VA, May 1991.

Wedge-Cone Waverider Configuration for Engine-Airframe Integration

Naruhisa Takashima* and Mark J. Lewis†
University of Maryland,
College Park, Maryland, 20742

Introduction

HYPERSONIC waveriders are promising shapes for the forebodies of engine-integrated hypersonic vehicles. These configurations can form the basis of airframes with very high lift-to-drag ratios (L/D). Furthermore, because they are designed with an inverse methodology, the flowfield is first selected, then the appropriate generating shape is determined; they lend themselves especially well to inlet optimization, as was shown by O'Neill and Lewis.[1] The resulting shapes provide relatively uniform inlet conditions, corresponding to the flow conditions of the original generating flow. O'Neill and Lewis integrated engines with a waverider forebody that were generated with a conical flowfield; a trailing-edge shape that defines the inlet curve was traced upstream from the inlet plane to carve the lower surface of the waverider. The shape was then optimized for maximum L/D by changing the shape of the trailing-edge curve and the shock angle. The center portion of the trailing-edge curve was fixed as an elliptical curve so that the difference in the normal distance between the shock and the surface in the spanwise direction could be minimized. This was done to allow the use of identical engine modules. Ideally, a circular arc instead of an elliptical curve should be used, however, this was shown to produce a waverider shape with potentially excessive aerodynamic heating in the nose and poor volumetric efficiency. By using an elliptical curve, the inlet flowfield will always have some nonuniformities. Also, because the generating flowfield is axisymmetric, there is a radially varying sidewash angle in the spanwise direction. The influence of the variation can be minimized by using multiple engine modules; however, each module will still experience flow nonuniformity in the radial direction.

Since these waverider inlet flow nonuniformities are a direct result of the conical nature of the design flowfield, it is of interest to examine other generating flowfields, particularly nonaxisymmetric shapes, for their ability to produce more uniform inlet properties. This work will focus on inlets derived from the flowfield associated with a hybrid wedge-cone combination.

Received Dec. 23, 1992; revision received May 3, 1994; accepted for publication Feb. 21, 1995.

*Graduate Research Assistant, Department of Aerospace Engineering. Student Member AIAA.

†Associate Professor, Department of Aerospace Engineering. Senior Member AIAA.

Generation of Wedge-Cone Waverider

With the exception of the osculating cones method of Sobieczky[2] and the use of the small-disturbance theory by Rasmussen,[3] waveriders have been generated with analytically defined flowfields, such as planar wedge flow and conical flows, or flowfields that are easily computed, such as by axisymmetric bodies. The advantages of using these types of generating bodies is that the flowfield behind the shock can be readily calculated, thereby allowing for quick design. This feature is especially important if the design is to be optimized, as multiple iterations may be required.

Such simple flowfields do have apparent limitations when the requirements on the waverider shape change from simple high lifting body to forebody design for hypersonic cruise vehicle. The need for high L/D, uniform flow at the inlet station, flat surfaces and high volume for ease of packaging and engine integration, and a desire for good off-design performance suggests that a more successful waverider might be constructed from a combination of different generating flowfields. For this study, a wedge-cone generating body was chosen with the expectation that the resulting waveriders would have the desirable characteristics of both planar wedge waveriders and conical waveriders: uniform flow at the inlet station from the planar region and high L/D with greater volume from the conical ends.

The wedge-cone body selected for this preliminary study has a width-to-length ratio of 0.25 and a cone semivertex angle of 7.5 deg. This cone angle is close to 7.09 deg, which is the semivertex angle of a pure cone that has been found to produce the maximum L/D for a 60-m-long waverider at Mach 6.[4]

The first step in designing a waverider shape is defining the generating flowfield. In the case of this wedge-cone waverider, an exact analytical solution is no longer available; instead, the flowfield has been calculated with CFL3D,[5] a three-dimensional Euler solver. The waverider shape was defined at freestream Mach number $M_\infty = 6$ and freestream unit Reynolds number $Re_{l\infty} = 2.157 \times 10^6$ (/m), which corresponds to a flight altitude of 30 km. The grid dimension was $101 \times 71 \times 51$ in the axial direction, circumferential direction, and radial direction, respectively. Figure 1 shows the calculated pressure contours on the generating wedge-cone body. Note that the actual calculation was done only on a quarter section using symmetric boundary conditions. The grid was adapted for pressure at each axial station using a method described by Hsu and Lytle.[6]

After the flowfield is calculated, a waverider can be generated from any stream surface in the region between the body and the shock. For a forebody design, the shape of the trailing edge curve that defines the lower surface contour at the inlet station will be dictated by the requirements of the propulsion system. The lower surface of the waverider is determined by tracing the streamlines along the trailing-edge curve upstream using a predictor-corrector method. Starting from the trailing-edge points, the location of the streamline is predicted on the axial plane immediately upstream. By taking an average of the velocity at the predicted location and the velocity at the previous plane, the corrected location is determined. The velocities are determined for each location by linearly interpolating the velocities at each grid point on the given axial plane. Each streamline is traced upstream until it intersects the shock surface. The shock surface was assumed to reside at the location of maximum pressure jump in the radial direction. The intersection between the stream surface and the shock then defines the leading-edge curve. The upper surface is taken to be a stream surface oriented in the freestream flow direction.

Figure 2 shows a waverider generated using the wedge-cone. Compared to the conical waveriders the nose of the vehicle is more spatulate. Table 1 presents the L/D, volume, and volumetric efficiency defined as (volume$^{2/3}$)/(total wetted area) of the waverider, as well as that of the conical Mach 6 optimized waverider. For both vehicles, the viscous effects were approximated using a reference temperature method for fully turbulent flow, and the vehicle length was chosen to be 60 m. Note that the the L/D value of this particular wedge-cone waverider compares quite favorably with that of the conical optimized waverider, even though the wedge-cone shape was not optimized for maximum L/D. At the same time the volume of the wedge-cone waverider is 80% greater than the conical waverider.

Computational Fluid Dynamics Validation

The design of the wedge-cone waverider was validated by solving the inviscid flowfield around the body using CFL3D. Figure 3 compares the pressure contours at the exit plane of the waverider shape to the pressure contours of the wedge-cone body. The computational solution indicates minor spillage at the leading edge due to shock detachment. This can be attributed to the fact that the exact shock location cannot

Table 1 Inviscid force coefficients and L/D for the wedge-cone waverider and Mach 6 viscous optimized waverider

	Wedge-cone	Mach 6	% Difference
L/D	7.260	7.738	−6.18
Volume, m^3	4180	2327	79.6
Volumetric efficiency	8.044E-2	5.988E-2	34.3

Table 2 Inviscid force coefficients and L/D for the wedge-cone waverider

	Design code	CFL3D	% Difference
C_L	5.624E-2	5.583E-2	0.734
C_D	6.334E-3	6.271E-3	1.00
L/D	8.879	8.893	−0.157

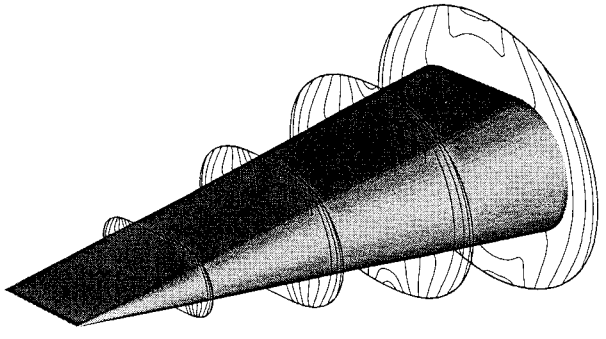

Fig. 1 Pressure contours about the wedge-cone generating body.

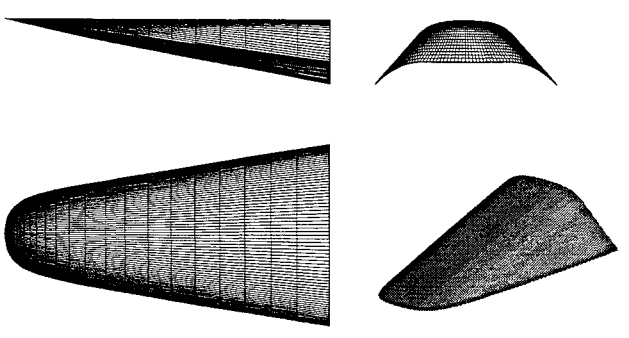

Fig. 2 Three-view and perspective view of the wedge-cone waverider.

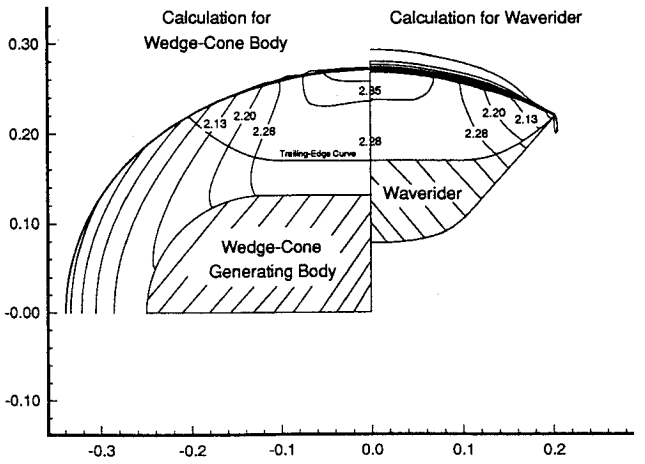

Fig. 3 Pressure contours at the exit plane.

be determined in the original generating flowfield. Despite this, excellent agreement is found between the original generating flowfield and the flowfield generated by the resulting waverider, a result that validates the design process. Also, as shown in Table 2, excellent agreement is found between the inviscid force coefficients calculated by the two methods.

Conclusions

This new class of waveriders, generated using a general nonaxisymmetric three-dimensional flowfield, shows great promise for engine-airframe integrated vehicles. This wedge-cone-derived body was found to better satisfy the requirements for forebody design than the more traditional conical waveriders. The design process was validated by calculating the flowfield about the waverider using a three-dimensional Euler solver. A high L/D value was obtained for this nonoptimized waverider, which suggests that waveriders might be optimized to produce even greater aerodynamic performance, while at the same time retaining the desirable inlet flow properties.

Because it requires a three-dimensional Euler solution, the current design process is time-consuming. Future work will focus on improving the method so that the shock location can be determined more precisely. The usage of a shock-fitting method is being considered. A reduction in generating time might be found by using an osculating-cone method, however, this current process has the advantage of providing all desired flowfield information of the generating flowfield at the beginning of the design.

References

[1]O'Neill, M. K., and Lewis, M. J., "Optimized Scramjet Integration on a Waverider," *Journal of Aircraft*, Vol. 29, No. 6, 1992, pp. 1114–1121.

[2]Sobieczky, H., Dougherty, F. C., and Jones, K. D., "Hypersonic Waverider Design from Given Shock Waves," *Proceedings of the First International Hypersonic Waverider Symposium*, Univ. of Maryland, College Park, MD, 1990.

[3]Rasmussen, M. L., "Waverider Configurations Derived from Inclined Circular and Elliptic Cones," *Journal of Spacecraft and Rockets*, Vol. 17, No. 6, 1980, pp. 537–545.

[4]Corda, S., and Anderson, J. D., Jr., "Viscous Optimized Hypersonic Waveriders Designed from Axisymmetric Flow Fields," AIAA Paper 88-0369, Jan. 1988.

[5]Vasta, V. N., Thomas, J. L., and Wedan, B. W., "Navier-Stokes Computations of Prolate Spheroids at Angle of Attack," AIAA Paper 87-2627, Aug. 1987.

[6]Hsu, A., and Lytle, J., "A Simple Algebraic Grid Adaptation Scheme with Applications to Two- and Three-Dimensional Problems," AIAA Paper 89-1984, April 1989.

Visualization of Choked Supersonic Flow-Through Engine Nacelles

Eddie Irani*
Wichita State University, Wichita, Kansas 67260-0044

Introduction

SUPERSONIC wind-tunnel models of complete aircraft are usually of small scale, due to the small size of most supersonic wind tunnels. The size of engine nacelles on wind-tunnel models of supersonic transport aircraft can be quite small, these nacelles thus operate at low Reynolds number. Often such nacelles are of the flow-through type and the low Reynolds number internal flow through these nacelles may cause substantial boundary-layer buildup, resulting in a choked flow condition. The choked internal flow will cause a detached bow shock on the nacelle that could adversely affect the flow on the model, leading to inaccurate flow structure predictions.[1]

The present tests were carried out to identify the flow about a particular truncated cone-type nacelle with a smooth, constant cross section, flow-through channel, and a sharp leading edge. The effects of choked flow through the nacelle on the surrounding flow were desired. In addition, it was hoped that any difference in exit flow structure between the choked and unchoked internal flow cases could be identified. Four configurations were considered, an unchoked internal flow, a frictionally choked internal flow, and two cases of physically restricting the flow through the nacelle. The nacelle was tested at Mach 1.94 and a model Reynolds number of 2.5×10^6. The nacelle was 63.5 mm long and had a length-to-i.d. ratio of 10.

Model Description

An axisymmetric supersonic engine nacelle-pylon model with a smooth, circular flow-through channel was designed and fabricated (Fig. 1a). The model had a constant diameter hole along the flow axis to simulate the flow channel. The nacelle was shaped as a truncated cone. It was 63.5 mm in length and had a flow-through channel diameter of 6.35 mm, giving a length-to-i.d. ratio of 10. Leading edges on the model were 0.025 mm thick. The pylon was extended and flared into a standard sting that attached to the tunnel C-mount. The axis of rotation for angle-of-attack changes was fixed relative to the tunnel and located at the leading edge of the model.

Four model configurations were tested. The first was the original unmodified model as described previously. The second was the original model coated on the inside wall with no. 80 grit to create a constant diameter channel with high friction, hence, causing friction-induced choked flow. Third, a 13-mm-long, 4.8-mm-i.d. tube was inserted in the smooth flow-through channel 6.5 mm downstream of the leading edge (Fig. 1b) to restrict the internal flow and obtain a detached bow shock. Fourth, a coarse nylon screen with 0.5-mm strands and about 50% porosity was added just upstream of the tube in the third configuration to further restrict the flow.

Facilities

The tests were carried out at Wichita State University's 230 by 230 mm test section supersonic wind tunnel. This is a blowdown facility in which the Reynolds number may be

Received May 24, 1993; revision received Sept. 21, 1994; accepted for publication Feb. 21, 1995.

*Graduate Research Assistant, Department of Aerospace Engineering. Member AIAA.